Dalton Transactions

Electrochemical behavior of a Rh(pentamethylcyclopentadienyl) complex bearing an NAD^+/NADH-functionalized ligand

Journal:	*Dalton Transactions*
Manuscript ID	DT-ART-12-2017-004594.R2
Article Type:	Paper
Date Submitted by the Author:	27-Feb-2018
Complete List of Authors:	Kobayashi, Katsuaki; Osaka City University, Department of Chemistry, Graduate School of Science Koizumi, Take-aki; Tokyo Institute of Technology, Chemical Resources Laboratory Ghosh, Debashis; Kyoto University, Institute for Cell-Material Sciences Kajiwara, Takashi; Kyoto Univ., Institute for Integrated Cell–Material Sciences (KUIAS/iCeMS) Kitagawa, Susumu; Kyoto University, Institute for Integrated Cell-Material Sciences Tanaka, Koji; Kyoto University, Institute for Integrated Cell-Material Sciences

Journal Name

ARTICLE

Electrochemical behavior of a Rh(pentamethylcyclopentadienyl) complex bearing an NAD$^+$/NADH-functionalized ligand

Received 00th January 20xx,
Accepted 00th January 20xx

DOI: 10.1039/x0xx00000x

www.rsc.org/

Katsuaki Kobayashi,[a]* Take-aki Koizumi,[b] Debashis Ghosh,[c] Takashi Kajiwara,[c] Susumu Kitagawa,[c] Koji Tanaka[c]*

A RhCp* (Cp* = pentamethylcyclopentadienyl) complex bearing an NAD$^+$/NADH-functionalized ligand, [RhCp*(pbn)Cl]Cl ([**1**]Cl, pbn = (2-(2-pyridyl)benzo[*b*]-1,5-naphthyridine)), was synthesized. The cyclic voltammogram of [**1**]Cl in CH_3CN shows two reversible redox waves at $E_{1/2}$ = −0.58 and −1.53 V (*vs*. the saturated calomel electrode (SCE)), which correspond to the Rh^{III}/Rh^{I} and pbn/pbn$^{\bullet-}$ redox couples, respectively. The addition of acetic acid to the solution afforded the proton-coupled two-electron reduction of [**1**]Cl at −0.62 V, from which [RhCp*(pbnHH)Cl]$^+$ was selectively generated, probably *via* a hydride transfer from a Rh^{III}–hydride intermediate to the pbn ligand. Complex [**1**]Cl is stable under acidic conditions, whereas a methyl proton of the Cp* moiety dissociates under basic conditions. The resulting anionic methylene group attacks the *para* carbon of the free pyridine of pbn, accompanied by protonation of the nitrogen atom of the ligand. As a result, treatment of [**1**]Cl with a base produces selectively the cyclic complex [**1CH**]Cl, which bears a reduced pbn framework (pbnCH). [**1CH**]Cl forms 1:1 adducts with $PhCOO^-$ *via* hydrogen bonding. A similar adduct, formed by a Ru-pbnHH scaffold and $RCOO^-$ (R = CH_3, C_6H_5), has been reported to react with CO_2 to produce $HCOO^-$ under concomitant regeneration of Ru-pbn. The adduct of [**1CH**]Cl with $PhCOO^-$, however, lacks such hydride-donor ability, due to a steric barrier in the molecular structure of [**1CH**]Cl, which hampers the hydride transfer.

Introduction

The NAD$^+$/NADH redox couple plays an essential role in hydride transfer processes (two electrons and one proton), enabling selective biomolecular transformations in a variety of biochemical redox reactions that do not produce any side products.[1-7] The development of renewable hydride reagents that do not generate any byproducts is considered one of the pillars toward a sustainable society. A variety of studies have been carried out to mimic the function of the NAD$^+$/NADH redox couple for applications in organic synthesis.[3, 8-18] However, the reversible conversion of NAD$^+$ and NADH models in redox reactions has so far been only rarely achieved.[14, 19-22]
We have previously reported two types of redox-active ligands aimed to mimic the NAD$^+$/NADH redox chemistry:[23-38] (i) a bipyridine (bpy)-based pbn ligand (Figure 1a)[23, 24, 28, 29, 39] and (ii) a 1,10-phenanthroline (phen)-based bpp compound (Figure 1b).[36] The resulting Ru-pbn and Ru-bpp complexes smoothly undergo photo-induced proton-coupled two-electron reductions that selectively afford the corresponding Ru-pbnHH[28, 29] and Ru-bppHH[36] complexes in the presence of sacrificial electron donors. Although the hydricity of such Ru-pbnHH and Ru-bppHH complexes is very low compared to that of inorganic hydrides (such as $NaBH_4$, NaH, or $LiAlH_4$), the hydride-donor ability of the Ru-pbnHH framework was greatly enhanced upon treatment with a strong base such as $RCOO^-$ (R = CH_3 or C_6H_5), whereafter Ru-pbnHH smoothly reacted with CO_2 to produce HCOOH under concomitant regeneration of Ru-pbn.[39] Conversely, the adduct of Ru-bppHH and a base was not able to reduce CO_2 in the presence of an excess of base, although it did function as a $2e^-/2H^+$ donor in the reduction of O_2, producing H_2O_2 under irradiation with visible light.[36] It should be noted that [Re(pbn)(CO)$_3$Cl] can also be reduced to [Re(pbnHH)(CO)$_3$Cl] under photo-irradiation,[40] similarly to the Ru-pbn[28, 29] and Ru-bpp[36] complexes, although the hydricity of such Re complexes has not yet been clarified.
The unique photo-character of polypyridyl Ru^{II} and Re^{I} complexes arises from metal-to-ligand charge-transfer (MLCT) processes in combination with other ligand-localized redox reactions. Under photo-irradiation, M-pbn complexes (M = Ru^{II}, Re^{I}) are smoothly reduced to M-pbnHH in the presence of a sacrificial electron donor. Judicious engineering of such M-

[a] *Department of Chemistry, Graduate School of Science, Osaka City University, Sumiyoshi-ku, Osaka 558-8585 Japan. E-mail: kobayash@sci.osaka-cu.ac.jp*
[b] *Laboratory for Chemistry and Life Science, Institute of Innovative Research, Tokyo Institute of Technology, 4259 Nagatsuta, Midori-ku, Yokohama 226-8503, Japan.*
[c] *Institute for Integrated Cell–Material Sciences (KUIAS/iCeMS), Kyoto University, Yoshida, Sakyo-ku, Kyoto 606-8501, Japan. E-mail: koji.tanaka@icems.kyoto-u.ac.jp*

Electronic Supplementary Information (ESI) available: ESI-MS spectrum of [**1**]Cl in CH_3CN containing 10% TEA; spectro-electrochemistry of $[RhCp^*(bpy)Cl]^+$; gradual changes in the cyclic voltammograms of [**1**]Cl in the presence of varying amounts of AcOH; ESI-MS spectrum of [**1**]Cl in the presence of 1.0% AcOH and 2 equiv. $CoCp_2$; and ^{1}H NMR spectra of [**1**]Cl, [**1CH**]Cl, and $[\mathbf{1HH}]^+$ generated by addition of $CoCp_2$ in the presence of excess acid. Crystallographic information files (cif) of [**1**][PF_6]·0.5(CH_3)$_2$CO and [**1CH**]Cl·2CH_3OH. CCDC 1565071 ([**1**][PF_6]·0.5(CH_3)$_2$CO) and 1565072 ([**1CH**]Cl·2CH_3OH). See DOI: 10.1039/x0xx00000x.

pbnHH complexes is an essential requisite for reversible organic hydride-donor reagents able to mimic the functions of the NAD^+/NADH redox couple. Very recently, it has been shown that one-electron injection into the ligand of a Ru-pbnHH complex results in hydride-donor properties toward the electrochemical reduction of CO_2.[41] Based on the aforementioned findings, the introduction of another redox center as an electron donor to metal-pbnHH complexes may provide a new pathway toward reversible hydride-donor catalysts. Considering the redox potentials of the pbn/pbnHH couple, the metal-centered reduction potentials of Ru-pbnHH and Re-pbnHH complexes are too negative for efficient coupling with the respective ligand-localized redox reactions. On the other hand, the reduction of Pd^{II}-pbn derivatives inevitably results in the deposition of Pd^0 particles due to the predominant reduction of the metal center.[25] Accordingly, Rh-pbn complexes seem reasonable prospectives to achieve reversible hydride-donor character on the basis of the redox potentials of the $Rh^{III/I}$ couple in Rh-polypyridyl complexes and those of the ligand-localized pbn/pbnHH couple in Ru complexes (−1.0 and −0.8 V *vs*. saturated calomel electrode (SCE), respectively).[21, 42-47] In addition, RhCp* complexes (Cp* = pentamethylcyclopentadienyl) that bear diimino or polypyridyl ligands are often used as asymmetric hydrogenation catalysts.[22,48,49-53] Indeed, Colbran *et al.* have proposed a hydride exchange between Rh and an NADH framework.[21, 22] Introduction of pbn into the RhCp* scaffold may therefore create synergistic effects that enhance the hydricity of the complex to mimic the NAD^+/NADH redox chemistry. This work describes the redox behavior of $[RhCp^*(pbn)Cl]^+$ ($[\mathbf{1}]^+$, Figure 1c) and its acid–base equilibria in H_2O and CH_3CN.

Results and discussion

Synthesis and X-ray structure of $[1]^+$

[RhCp*(pbn)Cl]Cl ([**1**]Cl) was prepared by a procedure similar to the synthesis of polypyridyl RhCp* complexes.[54, 55] A mixture of $[RhCp^*Cl_2]_2$ and two equivalents of pbn was stirred in EtOH for 1 h. During this time, the red suspension turned into a clear red/orange solution. After evaporation of the solvent under reduced pressure, the resulting residue was dissolved in CH_3CN, and a small amount of an insoluble product was removed by filtration. Concentration of the filtrate under reduced pressure afforded [**1**]Cl (74% yield), which is highly soluble in water, MeOH, EtOH, and CH_3CN. In CH_3CN, [**1**]Cl exhibits a strong electronic absorption band at 385 nm with two shoulders at 368 nm and 420 nm. The ^{1}H-NMR spectrum of [**1**]Cl in CD_3CN displays a characteristic singlet at 1.51 ppm, which should be assigned to the Me groups of Cp*, owing to the free rotation of the Cp* ring relative to the Rh atom. All the other NMR signals in the aromatic region correspond to the pbn ligand (Figure 2).

Suitable single crystals of the hexafluorophosphate salt of $[\mathbf{1}]^+$ ($[\mathbf{1}][PF_6]$) were subjected to X-ray diffraction analysis. The molecular structure of $[\mathbf{1}][PF_6]$ is shown in Figure 3a and selected bond lengths and angles are provided in Table 1. $[\mathbf{1}][PF_6]$ contains a facial Cp* moiety, with the pbn moiety in a vertical configuration and a monodentate Cl^- ligand. The bond lengths between the Rh center and the carbon atoms of the Cp* ring are 2.167(2), 2.152(2), 2.180(2), 2.208(3), and 2.163(3) Å, while the C–C bond lengths in the Cp* ring are almost equal (~1.43 Å). These data thus strongly suggest a η^5 coordination of the Cp* ligand.[46, 48, 49, 55] The C–C bond lengths of C15–C16 (1.395(3) Å) and C16-C17 (1.376(3) Å), as well as the bond angle around C16 in Figure 3a, *i.e*., the *para* carbon atom of the free pyridine moiety in pbn (C15–C16–C17: 120.1(2)°), indicate a ligand oxidation state consistent with an NAD^+/NADH-functionalized model.[23, 29]

Table 1 Selected bond lengths (Å) and angles (°) for $[\mathbf{1}][PF_6]$ and [**1CH**]Cl

	$[\mathbf{1}][PF_6]$	[**1CH**][Cl]
Rh1–Cl1	2.3971(8)	2.3819(10)
Rh1–N1	2.094(2)	2.092(3)
Rh1–N2	2.1339(19)	2.086(3)
Rh1–C18	2.208(3)	2.132(4)
Rh1–C19	2.180(2)	2.164(4)
Rh1–C20	2.152(2)	2.161(4)
Rh1–C21	2.167(2)	2.166(4)
Rh1–C22	2.163(3)	2.137(4)
C18–C19	1.414(4)	1.428(5)
C19–C20	1.446(4)	1.449(5)
C20–C21	1.420(4)	1.439(5)
C21–C22	1.433(4)	1.440(5)
C18–C22	1.436(4)	1.456(6)
C15–C16	1.395(3)	1.520(6)
C16–C17	1.376(3)	1.510(6)
N3–C10	1.347(3)	1.382(6)
N3–C9	1.344(3)	1.363(6)
C10–C15	1.440(4)	1.405(6)
C9–C17	1.432(3)	1.403(6)
N3–C10–C15	122.8(2)	121.0(4)
C10–C15–C16	117.7(2)	120.9(4)
C15–C16–C17	120.1(2)	110.7(4)
C16–C17–C9	118.2(2)	122.4(4)
C17–C9–N3	123.2(2)	120.2(4)
C9–N3–C10	117.8(2)	121.6(4)

Acid–base behavior of [1]Cl

[**1**]Cl is soluble in water, and the acid–base equilibrium of the free nitrogen atom on pbn was examined to evaluate the basicity of the ligand.[24] Figure 4 shows the spectral changes for [**1**]Cl at different pH values in water. The absorption band at 382 nm gradually decreases with increasing pH starting at pH = 2.0 (Figure 4a). These spectral changes were almost reversible between pH = 2.0 and pH = 8.0. In contrast, at pH > 10, new bands gradually appear at 350 and 430 nm (Figure 4b); thereafter, the original spectrum of [**1**]Cl cannot be recovered upon acidification of the medium. Thus, [**1**]Cl should undergo irreversible structural changes under strongly basic conditions. The rate of spectral variation increased with the pH value. The NMR and ESI-MS spectra of [**1**]Cl in strongly alkaline aqueous

solution revealed the fragmentation of the complex into several species.

The absorption spectrum of [**1**]Cl in CH_3CN changed rapidly after addition of triethylamine (TEA; Figure 5) compared to the rate of spectral changes for the complex in strongly alkaline aqueous solution. The features of the spectrum in the presence of TEA in CH_3CN closely resemble those in strongly alkaline solution, and do not reverse to the original ones upon acidification using *e.g*. acetic or trifluoroacetic acid. It is worth noting that, despite the stark differences in the absorption spectra before and after treatment of [**1**]Cl with TEA in CH_3CN, the ESI-MS spectrum in the presence of TEA was identical to that of the original complex (Figure S1). The base-treated complex ([**1CH**]Cl) was subsequently isolated from a CH_3CN/TEA (9:1) solution. The NMR spectrum of [**1CH**]Cl in CD_3CN exhibits four non-equivalent singlet signals with 3H intensity at 1.5–2.1 ppm (Figure 6). This observation indicates that [**1CH**]Cl contains four non-equivalent methyl groups in the Cp* moiety, possibly due to suppression of the free rotation of Cp* and the loss of one of the Me groups. In addition, methylene peaks with geminal coupling emerged at 2.49 and 2.88 ppm, together with a methine signal at 4.97 ppm. In the aromatic region, the singlet signal of [**1**]Cl at 9.48 ppm disappeared completely after addition of the base; instead, one broad singlet peak was observed at 10.12 ppm, which was assigned to an NH proton. These NMR observations suggest that one of the methyl groups has been transformed into a methylene moiety, and the appearance of an NH proton indicates the formation of a pbnHH framework.

Single crystals of [**1CH**]Cl were obtained by slow diffusion of Et_2O into a methanolic solution of [**1CH**]Cl. The corresponding X-ray crystal structure is shown in Figure 3b and selected bond lengths and angles are summarized in Table 1. [**1CH**]Cl presents a cyclic structure generated by the formation of a C–C bond between one of the Me groups of Cp* and the *para* carbon atom of the functional pyridine moiety of pbn (Cp'-pbnH or pbnCH). The η^5-Cp* binding mode of [**1**]Cl is maintained in [**1CH**]Cl. The shortening of the Rh–C18 bond in [**1CH**]Cl (2.132(4) Å) compared to that in [**1**][PF_6] (2.208(3) Å) was ascribed to the position of C18 in Figure 3b, which is bound to the methylene group and connecting the Cp* and pbn ligands. The reactive carbon atom of pbn (C16) in [**1CH**]Cl exhibits an sp^3 configuration; the C15–C16 and C16–C17 bond distances are 1.520(6) and 1.510(6) Å, respectively. The C15–C16–C17 bond angle of 110.7(4)° is the narrowest among the Ru-pbnHH analogues reported so far.[24, 29, 36, 37] The C10–C15 and C9–C17 bond distances in [**1CH**]Cl are slightly shorter than those in [**1**][PF_6]. Moreover, the N3–C9 and N3–C10 distances increased after the transformation of [**1**]Cl into [**1CH**]Cl. These structural characteristics are consistent with a dihydropyridine framework in the pbnHH ligand of Ru-pbnHH.[24, 29, 36, 37]

Based on the aforementioned observations, the most likely pathway from [**1**]Cl to [**1CH**]Cl is depicted in Scheme 1. Treatment of [**1**]Cl with a base should induce the deprotonation of one of the methyl groups of the $Rh^{III}Cp^*$ framework, and the subsequent nucleophilic attack of the resultant carbanion should occur on the electron-deficient pyridine ring of pbn.

Electrochemical properties of [1]Cl

The cyclic voltammogram of [**1**]Cl is shown in Figure 7a. Two reversible and one pseudo-reversible redox couples are observed at −1.53, −0.58, and 0.95 V (all voltages *vs*. SCE), respectively. Based on the assignment for $[RhCp^*(bpy)Cl]^+$ in CH_3CN,[43, 46] the redox couples at −0.58 V and −1.53 V were assigned to the $Rh^{III/I}$ couple under concomitant release of Cl^- (eq. 1) and the pbn/$pbn^{\bullet-}$ couple, respectively. The irreversible anodic wave corresponds most likely to the oxidation of Rh^{III} to Rh^{IV}.[56]

$$Rh^{III}\text{–}Cl + 2e^- \rightleftharpoons Rh^{I} + Cl^- \qquad (1)$$

As mentioned above, [**1**]Cl exhibits an absorption maximum at 385 nm with two shoulders in its electronic absorption spectrum. The electrochemical reduction of [**1**]Cl at −1.0 V involves two electrons per molecule, accompanied by the appearance of two strong absorption bands at 619 and 816 nm (Figure 8a). Similar spectral changes were observed for the electrochemical reduction of [RhCp*(bpy)Cl]Cl (Figure S2).[57] Thus, the −0.58 V redox reaction of [**1**]Cl can be reasonably assigned to the Rh^I/Rh^{III} couple (eq. 1).

The cyclic voltammogram of [**1**]Cl in the presence of excess TEA displays one pseudo-reversible redox wave at –0.88 V. The pattern is the same as that obtained for isolated [**1CH**]Cl (*vide infra*). The addition of AcOH to [**1**]Cl in CH_3CN resulted in a gradual positive (anodic) shift of the pbn/$pbn^{\bullet-}$ couple due to a proton-coupled electron-transfer (PCET) process (Figure S3). Moreover, in the presence of 10 equiv. of AcOH, [**1**]Cl exhibits two irreversible cathodic waves at −0.62 and −0.87 V, and a new anodic wave at 0.53 V (Figure 7b). Further addition of AcOH did not result in further changes of the CV curve. As expected for the PCET redox process of Ru-pbn complexes, the irreversible anodic wave at 0.53 V is coupled to the cathodic wave at −0.62 V.

Indeed, the electrochemical reduction of [**1**]Cl in the presence of 10 equiv. of AcOH at −0.76 V, *i.e.*, an intermediate potential between the first and second cathodic waves, was not accompanied by any absorption bands correlated with Rh^I species in the range of 600–800 nm, although a small bathochromic shift of the original absorption band was observed (Figure 8b). Upon electrochemical oxidation of the resulting solution at 0.6 V, the original absorption spectrum was fully recovered. Further electrochemical reduction of $[\mathbf{1}]^+$ conducted at –1.0 V in the presence of 10 equiv. of AcOH induced a gradual reduction of the absorption band intensity. This behavior is quite similar to that of $[RhCp^*(bpy)Cl]^+$ in the presence of an acid, indicating that the secondary reduction of [**1**]Cl under acidic conditions proceeds *via* a fragmentation process similar to that of $[RhCp^*(bpy)Cl]^+$. In other words, the reduction of $[RhCp^*(bpy)Cl]^+$ should generate a Rh^{III}–H species *via* the protonation of Rh^I (eq. 2).[54, 57, 58] Further reduction under acidic conditions likely results in the decomposition of

Rh^{III}–H (eq. 3) or the evolution of H_2 by reaction with H^+ (eq. 4).[43, 54, 57]

$$Rh^{I} + H^{+} \rightarrow Rh^{III}–H \quad (2)$$
$$Rh^{III}–H + 2e^{-} \rightarrow Rh^{I} + H^{-} \quad (3)$$
$$Rh^{III}–H + H^{+} + Cl^{-} \rightarrow Rh^{III}–Cl + H_2 \quad (4)$$

Chemical reduction of [1]Cl in acidic medium

The reduction of [**1**]Cl was carried out using $CoCp_2$ in acidic medium by exploiting the redox potential of the $[CoCp_2]/[CoCp_2]^+$ couple. The electronic absorption spectrum of [**1**]Cl in the presence of 2 equiv. of $CoCp_2$ in CH_3CN containing 1.0% AcOH (Figure S4) was consistent with that of the electrochemical reduction of [**1**]Cl at -1.0 V in acidic medium (Figure 8b). The ^{1}H NMR spectrum of [**1**]Cl also clarified the selective reduction of the pbn ligand in the same acidic CD_3CN in place of CH_3CN (Figure 9).[59] The characteristic peaks of the methylene group of pbnHH were observed at 4.43 ppm with geminal coupling (J = 21.0 Hz),[28, 29, 36] and the pattern of the aromatic region also supports the formation of a pbnHH framework. The ESI-MS spectrum of the solution showed the presence of $[RhCp^*(pbnHH)Cl]^+$ ([**1HH**]$^+$) and a small peak for [**1**]$^+$ (Figure. S5). It can therefore be concluded that [**1**]$^+$ is selectively reduced to [**1HH**]$^+$ under electrolysis at −0.76 V (eq. 5), and that [**1**]$^+$ is regenerated by oxidation of [**1HH**]$^+$ at 0.53 V (eq. 6).

$$[\mathbf{1}]^{+} + 2\,H^{+} + 2\,e^{-} \rightarrow [\mathbf{1HH}]^{+} \quad (5)$$
$$[\mathbf{1HH}]^{+} \rightarrow [\mathbf{1}]^{+} + 2\,H^{+} + 2\,e^{-} \quad (6)$$

There are two possible pathways for the formation of [**1HH**]$^+$ *via* the two-electron reduction of [**1**]$^+$ under acidic conditions (eq. 5). The first one involves a metal-centered two-electron reduction of [**1**]$^+$ under concomitant dissociation of Cl^- (eq. 1), followed by a proton attack on the Rh^I center, which would afford a Rh^{III}–H complex (Scheme 2a). Hydride transfer from Rh^{III}–H to the reactive carbon atom of pbn (C16 in Figure 3), accompanied by protonation of the nitrogen atom, would then furnish the pbnHH framework. Recombination of Cl^- with the Rh^{III} center should then facilitate an intramolecular hydride transfer. Similar hydride transfer processes from M–H to NAD^+-model compounds have been described for Rh[21, 22] and Ru[37] complexes.[14] The second pathway involves a pbn-localized reduction that occurs primarily prior to the metal-centered reduction, as suggested by the significant anodic shift of the redox potential of the ligand caused by such a PCET process (Scheme 2b). The one-electron reduction of the pbn ligand greatly increases the basicity of the nitrogen atom, whose spontaneous protonation forms the neutral radical pbnH$^\bullet$. The intermolecular π–π assembly of two neutral pbnH$^\bullet$ radicals would then generate dimeric $\{[Cp^*Rh(pbnH^\bullet)Cl]\}_2^{2+}$, in which intramolecular $1e^-/1H^+$ transfer between two pbnH$^\bullet$ radicals should induce its disproportionation into the Rh-pbn and Rh-pbnHH complexes, as reported for the photochemical two-electron reduction of Ru-pbn complexes.[27–29] Despite numerous attempts to isolate [**1HH**]$^+$, we have so far been unsuccessful due to its high sensitivity toward air. Yet, the structural and electrochemical properties of [**1HH**]$^+$ are currently under investigation and will be reported in due course.

Electrochemical properties of [1CH]Cl

The cyclic voltammogram of [**1CH**]Cl shows a pseudo-reversible redox couple at −0.88 V and two irreversible peaks at 1.06 and 1.28 V (Figure. 10a). The −0.88 V peak was assigned to the Rh^{III}/Rh^I couple based on the assignment of the cyclic voltammogram of [**1**]Cl. One of the irreversible anodic waves probably originates from the oxidation of Rh^{III}, while the other should be correlated to the oxidation of the cyclic Cp'-pbnH (pbnCH) framework.[29] The anodic peak of [**1CH**]Cl at 1.06 V shifts to 0.52 V upon addition of $PhCOO^-$ (Figure 10b), due to the formation of an adduct between the N–H proton of [**1CH**]Cl and $PhCOO^-$ (Figure 11), similar to the case of the N–H proton of Ru-pbnHH and $RCOO^-$ (R = CH_3 or C_6H_5), whose hydrogen bonding induced a substantial cathodic shift of the oxidation potential of the adduct. Indeed, the broad N–H proton signal in the NMR spectrum of [**1CH**]Cl centered at 10.0 ppm shifted to lower magnetic field (12.97 ppm) upon addition of $PhCOO^-$ (Figure 12).[39, 60] The 1:1 adducts of Ru-pbnHH and $RCOO^-$ (R = CH_3 or C_6H_5) effectively enhance the hydricity of pbnHH, which smoothly reacts with CO_2 to produce $HCOO^-$ and Ru-pbn in dry CH_3CN.[39] However, [**1CH**]Cl remained unchanged in the presence of an excess of $PhCOO^-$ in CH_3CN under CO_2. Thus, the hydricity of [**1CH**]Cl was not enhanced by the formation of an adduct with $PhCOO^-$. It is worth noting that the hydride transfer from Ru-pbnHH to CO_2 is usually accompanied by a configurational change from an sp^3 hybridization of the *para* carbon of NADH moiety in Ru-pbnHH (C16) to an sp^2–hybridized Ru-pbn framework.[24,29,36,37] The lack of such a hydride-donor ability of [**1CH**]Cl in the presence of $PhCOO^-$ is therefore ascribed to the difficulties associated with the required configurational change of the sp^3-hybridized orbital of C16 in cyclic [**1CH**]Cl to a planar sp^2-hybridized orbital. In other words, cyclic [**1CH**]Cl does not seem to be a suitable hydride-donation catalyst compared to non-cyclic Ru-pbnHH on account of the hampered configurational change from sp^3 to sp^2 hybridization at the active reaction site.

Conclusions

In contrast to the redox behavior of Ru-pbn complexes, [RhCp*(pbn)Cl]Cl ([**1**]Cl) undergoes not only pbn-localized but also Rh-centered redox reactions in CH_3CN at $E_{1/2}$ = −1.53 and −0.58 V, respectively. Upon addition of an acid to the solution, the ligand-localized reduction of [**1**]Cl shifts toward a more positive potential compared to the metal-centered reduction, indicating the proton-coupled reduction of pbn to produce a pbnHH moiety. The electrochemical and chemical reduction of [**1**]Cl in the presence of an acid selectively affords a Rh-pbnHH framework ([**1HH**]$^+$). [**1**]Cl is stable in acidic media, while the proton of the Cp* methyl group dissociates under basic conditions. An intramolecular attack of the resulting anionic

methylene moiety to the *para* carbon atom of the free pyridine moiety of pbn (C16 in Figure 3), followed by protonation of the pbn nitrogen atom, affords cyclic [**1CH**]Cl.

Although the orbital of the reactive carbon atom in pbn and pbnHH (C16) formally exhibits sp^2 and sp^3 hybridization, not only pbn but also pbnHH display an almost planar ring structure in the corresponding Ru complexes. A small configurational change at the functional carbon atom of the Ru-pbn and Ru-pbnHH skeletons facilitates the release of the hydride from the latter. Conversely, [**1CH**]Cl, which bears a tethered pbnCH ligand, is not suitable as a hydride-donor catalyst, given the strain to adopt such a planar sp^2-hybridization at the same position of the oxidized ligand. The lack of hydride donor ability of [**1CH**]Cl even upon formation of an adduct with $PhCOO^-$ should arise from a large structural barrier at the active center between the reduced and oxidized forms. Thus, the present work provides important guidelines for the design of NADH models for reversible hydride catalysis.

Experimental Section

Materials

$[RhCp^*Cl_2]_2$[61] and pbn[23] were prepared according to previously reported procedures, while [nBu$_4$N][PF$_6$] was purchased from Tokyo Chemical Industry Co., Ltd. and recrystallized from EtOH prior to use.

Preparation of [RhCp*(pbn)Cl]Cl ([1]Cl)

$[RhCp^*Cl_2]_2$ (300 mg, 0.46 mmol) and pbn (250 mg, 0.97 mmol) were dissolved in EtOH (50 mL) and stirred at room temperature for 1.5 h. After removal of the solvent under reduced pressure, the obtained residue was dissolved in CH_3CN (100 mL). The remaining insoluble phase was removed by filtration, and the solvent of the filtrate was evaporated under reduced pressure to afford a brown solid. This solid was then washed with Et_2O and finally dried *in vacuo*. Yield: 385 mg (74%). Single crystals suitable for X-ray diffraction analysis were obtained from the slow diffusion of Et_2O into an acetonitrile solution of [**1**][PF$_6$], which was prepared from [**1**]Cl by counter-ion exchange using a CH_3CN/H_2O mixture containing excess [NH$_4$][PF$_6$]. ESI-MS: m/z 530.03. Anal. calcd for $C_{27}H_{26}N_3Cl_2Rh\cdot 2.5H_2O$: C 53.04, H 4.96, N 6.88; found C 53.04, H 5.11, N 6.87. ^{1}H NMR (400 MHz, CD_3CN): δ 9.47 (s, 1H), 9.04 (d, J = 5.5 Hz, 1H), 8.95 (d, J = 9.2 Hz, 1H), 8.78 (d, J = 9.2 Hz, 1H), 8.72 (d, J = 8.2 Hz, 1H), 8.41-8.30 (m, 3H), 8.06 (t, J = 8.0 Hz, 1H), 7.93 (t, J = 6.6 Hz, 1H), 7.85 (t, J = 7.6 Hz, 1H), 1.51 (s, 15H) ppm.

Preparation of [Rh(Cp'-pbnH)Cl]Cl ([1CH]Cl)

[**1**]Cl (100 mg, 0.101 mmol) was dissolved in 10 mL of CH_3CN/TEA (9:1). The mixture was stirred for 3 h, after which a yellow solid precipitated. Removal of the solvent under reduced pressure afforded a yellow solid, which was washed with Et_2O and dried under reduced pressure. Yield: quant. ESI-MS: m/z 530.03. ^{1}H NMR (400 MHz, CD_3CN): δ 10.13 (d, J = 12.8 Hz, 1H), 8.73 (d, J = 5.5 Hz, 1H), 8.11-8.04 (m, 2H), 8.02 (d, J = 9.2 Hz, 1H), 7.73 (d, J = 8.7 Hz, 1H), 7.56 (td, J = 5.8, 2.6 Hz, 1H), 7.41 (d, J = 7.8 Hz, 1H), 7.22 (t, J = 7.6 Hz, 1H), 7.09 (d, J = 8.2 Hz, 1H), 7.01 (t, J = 7.4 Hz, 1H), 4.97 (dd, J = 11.9, 2.7 Hz, 1H), 2.88 (dd, J = 14.4, 12.1 Hz, 1H), 2.49 (dd, J = 14.2, 2.7 Hz, 1H), 2.09 (s, 3H), 1.87 (s, 3H), 1.64 (s, 3H), 1.16 (s, 3H) ppm.

Instruments

UV-vis spectra were recorded on an Agilent 8453 spectrometer. NMR spectra were recorded on a JEOL ECS-400 spectrometer, while ESI-MS spectra were obtained from a Waters Micromass LCT spectrometer.

Electrochemistry

Electrochemical measurements were conducted on an ALS/chi Model 660A electrochemical analyzer. Electrochemical experiments were performed using solutions of the complexes (1.0 mM) in CH_3CN containing 0.1 M [nBu$_4$N][PF$_6$]. A glassy carbon electrode, Ag/AgNO$_3$ (0.01 M), and a platinum wire were employed as the working, reference, and counter electrode, respectively. Spectro-electrochemistry analyses were performed in a thin-layer cell (optical length: ~0.05 cm), in which a platinum-mesh working electrode was inserted. A platinum wire and Ag/AgNO$_3$ (0.01 mM AgNO$_3$ in 0.1 M [nBu$_4$N][BF$_4$] in CH_3CN) were used as the counter and reference electrode, respectively. The cell was inserted in a spectrometer (Agilent 8453) to monitor the spectral changes during electrolysis.

X-ray crystallographic analysis

Crystals were mounted on loops and placed under N_2 stream at 163 K and 113 K, for [**1**][PF$_6$] and [**1CH**]Cl, respectively. X-ray diffraction data were collected on a Rigaku Saturn CCD area detector using graphite monochromatic Mo-$K\alpha$ radiation (λ = 0.71070 Å) and processed using the Crystal Clear software package (Rigaku). Structures were solved by a direct method, using SHELXT 2014/5,[62,63] and expanded using Fourier techniques. Non-hydrogen atoms were refined anisotropically by the full-matrix-least-squares method on F^2 using SHELXL 2014/7.[62, 63] All hydrogen atoms are located in their idealized positions (methyl C–H bond length: 0.98 Å; aromatic C–H bond length: 0.95 Å) and included in the structure calculations without further refinement of the parameters; crystallographic data are summarized in Table 2.

Conflicts of interest

There are no conflicts to declare.

Acknowledgements

K.K. acknowledges the Japanese Ministry of Education, Science, Sports, and Culture (MEXT) for a Grant-in-Aid for Scientific Research (26410017). S.K. acknowledges the Japan Science and Technology Agency (JST) for the Advanced Catalytic Transformation Program for Carbon Utilization (ACT-

C, JPMJCR12YB). K.T. acknowledges MEXT for a Grant-in-Aid for Scientific Research (26288024). This work was partially supported by the Cooperative Research Program of the "Network Joint Research Center for Materials and Devices".

Table 2 Crystallographic data for [**1**][PF_6]·0.5(CH_3)$_2$CO and [**1CH**]Cl·2CH_3OH

	[**1**][PF_6]·0.5(CH_3)$_2$CO	[**1CH**]Cl·2CH_3OH
Formula	$C_{28.5}H_{29}F_6N_3O_{0.5}PRh$	$C_{29}H_{32}Cl_2N_3O_2Rh$
Formula weight	704.88	628.38
Color	Orange	Orange
Crystal size / mm	0.30 × 0.20 × 0.10	0.20 × 0.10 × 0.04
Crystal system	Monoclinic	Monoclinic
Space group	*C*2/*c*	$P2_1/c$
a / Å	23.9844(31)	13.4222(26)
b / Å	17.8044(20)	14.4974(26)
c / Å	13.8845(23)	14.0871(26)
α / (°)	90	90
β / (°)	104.0178(71)	96.3341(8)
γ / (°)	90	90
V / Å^3	5752.5(1)	2724.43(0)
Z	8	4
T / K	163	113
ρ_c / g cm^{-3}	1.628	1.537
F(000)	2848	1296
Total reflections	22281	18584
Unique reflections (R_{int})	6582 (0.0316)	5548 (0.0311)
Refln. / Param. ratio	17.69	16.52
R_1[a] ($I > 2.00\sigma(I)$)	0.0379	0.0467
wR_2[b] (all data)	0.0937	0.1140
GOF on F^2	1.082	1.115

[a] $R_1 = \Sigma||F_o| - |F_c||/\Sigma|F_o|$. [b] $wR_2 = [\Sigma\{w(F_o^2 - F_c^2)^2\}/\Sigma w(Fo^2)^2]^{1/2}$.

Notes and references

1 U. Eisner and J. Kuthan, *Chem. Rev.*, 1972, **72**, 1-42.
2 P. L. Dutton and D. F. Wilson, *Biochim. Biophys. Acta*, 1974, **346**, 165-212.
3 D. M. Stout and A. I. Meyers, *Chem. Rev.*, 1982, **82**, 223-243.
4 B. Sunil, S. K. Talla, V. Aswani and A. S. Raghavendra, *Photosynth. Res.*, 2013, **117**, 61-71.
5 L. M. Lassen, A. Z. Nielsen, B. Ziersen, T. Gnanasekaran, B. L. Møller and P. E. Jensen, *ACS Synth. Biol.*, 2014, **3**, 1-12.
6 C. S. Silva, W. D. Seider and N. Lior, *Chem. Eng. Sci.*, 2015, **130**, 151-171.
7 D. S. Bilan, A. G. Shokhina, S. A. Lukyanov and V. V. Belousov, *Russ. J. Bioorg. Chem.*, 2015, **41**, 341-356.
8 C. Walsh, *Acc. Chem. Res.*, 1980, **13**, 148-155.
9 S.-L. You, *Chem. Asian J.*, 2007, **2**, 820-827.
10 S. G. Ouellet, A. M. Walji and D. W. C. MacMillan, *Acc. Chem. Res.*, 2007, **40**, 1327-1339.
11 C. Zheng and S.-L. You, *Chem. Soc. Rev.*, 2012, **41**, 2498-2518.
12 W. Du and Z. Yu, *Synlett*, 2012, **23**, 1300-1304.
13 F. Shi and L.-Z. Gong, *Angew. Chem. Int. Ed.*, 2012, **51**, 11423-11425.
14 A. McSkimming and S. B. Colbran, *Chem. Soc. Rev.*, 2013, **42**, 5439-5488.
15 G. Hamasaka, H. Tsuji and Y. Uozumi, *Synlett*, 2015, **26**, 2037-2041.
16 K.-H. Kim, C.-Y. Lee and C.-H. Cheon, *J. Org. Chem.*, 2015, **80**, 6367-6374.
17 F. Foubelo and M. Yus, *Chem. Rec.*, 2015, **15**, 907-924.
18 18. T. Ghosh, T. Slanina and B. König, *Chem. Sci.*, 2015, **6**, 2027-2034.
19 B. W. Cohen, D. E. Polyansky, R. Zong, H. Zhou, T. Ouk, D. E. Cabelli, R. P. Thummel and E. Fujita, *Inorg. Chem.*, 2010, **49**, 8034-8044.
20 A. McSkimming, M. Bhadbhade and S. B. Colbran, *Dalton Trans.*, 2010, **39**, 10581-10584.
21 A. McSkimming, M. M. Bhadbhade and S. B. Colbran, *Angew. Chem. Int. Ed.*, 2013, **52**, 3411-3416.
22 A. McSkimming, B. Chan, M. M. Bhadbhade, G. E. Ball and S. B. Colbran, *Chem.-Eur. J.*, 2015, **21**, 2821-2834.
23 T.-a. Koizumi and K. Tanaka, *Angew. Chem. Int. Ed.*, 2005, **44**, 5891-5894.
24 D. Polyansky, D. Cabelli, J. T. Muckerman, E. Fujita, T.-a. Koizumi, T. Fukushima, T. Wada and K. Tanaka, *Angew. Chem. Int. Ed.*, 2007, **46**, 4169-4172.
25 H. Tannai, T.-a. Koizumi and K. Tanaka, *Inorg. Chim. Acta*, 2007, **360**, 3075-3082.
26 M. Kimura and K. Tanaka, *Angew. Chem. Int. Ed.*, 2008, **47**, 9768-9771.
27 D. E. Polyansky, D. Cabelli, J. T. Muckerman, T. Fukushima, K. Tanaka and E. Fujita, *Inorg. Chem.*, 2008, **47**, 3958-3968.
28 T. Fukushima, E. Fujita, J. T. Muckerman, D. E. Polyansky, T. Wada and K. Tanaka, *Inorg. Chem.*, 2009, **48**, 11510-11512.
29 T. Fukushima, T. Wada, H. Ohtsu and K. Tanaka, *Dalton Trans.*, 2010, **39**, 11526-11534.
30 S. K. Padhi, K. Kobayashi, S. Masuno and K. Tanaka, *Inorg. Chem.*, 2011, **2011**, 5321-5323.
31 S. K. Padhi and K. Tanaka, *Inorg. Chem.*, 2011, **50**, 10718-10723.
32 S. K. Padhi, R. Fukuda, M. Ehara and K. Tanaka, *Inorg. Chem.*, 2012, **51**, 8091-8102.
33 S. K. Padhi, R. Fukuda, M. Ehara and K. Tanaka, *Inorg. Chem.*, 2012, **51**, 5386-5392.
34 K. Kobayashi and K. Tanaka, *Phys. Chem. Chem. Phys.*, 2014, **16**, 2240-2250.
35 T. Fukushima, R. Fukuda, K. Kobayashi, G. F. Caramori, G. Frenking, M. Ehara and K. Tanaka, *Chem.-Eur. J.*, 2015, **21**, 106-110.
36 K. Kobayashi, H. Ohtsu, K. Nozaki, S. Kitagawa and K. Tanaka, *Inorg. Chem.*, 2016, **55**, 2076-2084.
37 T. Fukushima, D. Ghosh, K. Kobayashi, H. Ohtsu, S. Kitagawa and K. Tanaka, *Inorg. Chem.*, 2016, **55**, 11613-11616.
38 D. Ghosh, T. Fukushima, K. Kobayashi, S. Sen, S. Kitagawa, T. Kato and K. Tanaka, *Dalton Trans.*, 2017, **46**. 4373–4381.
39 H. Ohtsu and K. Tanaka, *Angew. Chem. Int. Ed.*, 2012, **51**, 9792-9795.
40 Y. Matsubara, S. E. Hightower, J. Chen, D. C. Grills, D. E. Polyansky, J. T. Mucherman, K. Tanaka and E. Fujita, *Chem. Commun.*, 2014, **50**, 728-730.
41 D. Ghosh, K. Kobayashi, T. Kajiwara, S. Kitagawa and K. Tanaka, *Inorg. Chem.*, 2017, **56**, 11066-11073.
42 S. Chardon-Noblat, I. M. F. d. Oliveira, J.-C. Moutet and S. Tingry, *J. Mol. Catal. A: Chem.*, 1995, **99**, 13-21.
43 C. Caix, S. Chardon-Noblat, A. Deronzier, J.-C. Moutet and S. Tingry, *J. Organomet. Chem.*, 1997, **540**, 105-111.
44 J.-C. Moutet, C. Duboc-Toia, S. Ménage and S. Tingry, *Adv. Mater.*, 1998, **10**, 665-667.
45 J.-C. Moutet, L. Y. Cho, C. Duboc-Toia, S. Ménage, E. C. Riesgo and R. P. Thummel, *New J. Chem.*, 1999, **23**, 939-944.
46 W.-H. Wang, Y. Suna, Y. Himeda, J. T. Muckerman and E. Fujita, *Dalton Trans.*, 2013, **42**, 9628-9636.
47 Y. Hu and J. R. Norton, *J. Am. Chem. Soc.*, 2014, **136**, 5938-5948.

48 K. Mashima, T. Abe and K. Tani, *Chem. Lett.*, 1998, 1199-1200.
49 K. Murata, T. Ikariya and R. Noyori, *J. Org. Chem.*, 1999, **64**, 2186-2187.
50 Y. Himeda, N. Onozawa-Komatsuzaki, H. Sugihara, H. Arakawa and K. Kasuga, *J. Mol. Catal. A: Chem.*, 2003, **195**, 95-100.
51 M. Ito, Y. Endo, N. Tejima and T. Ikariya, *Organometallics*, 2010, **29**, 2397-2399.
52 L. Tang, Z. Lin, Q. Wang, X. Wang, L. Cun, W. Yuan, J. Zhu and J. Deng, *Tetrahedron Lett.*, 2012, **53**, 3828-3830.
53 C. L. Pitman, O. N. Finster and A. J. M. Miller, *Chem. Commun.*, 2016, **52**, 9105-9108.
54 U. Kölle and M. Grätzel, *Angew. Chem.*, 1987, **99**, 572-574.
55 L. Dadci, H. Elias, U. Frey, A. Hörnig, U. Koelle, A. E. Merbach, H. Paulus and J. S. Schneider, *Inorg. Chem.*, 1995, **34**, 306-315.
56 S. K. Singh, M. Trivedi, M. Chandra and D. S. Pandey, *J. Organomet. Chem.*, 2005, **690**, 647-652.
57 M. Ladwig and W. Kaim, *J. Organomet. Chem.*, 1992, **439**, 79-90.
58 M. Ladwig and W. Kaim, *J. Organomet. Chem.*, 1991, **419**, 233-243.
59 Further addition of $CoCp_2$ (up to 4 equiv.) to the acidic solution of $[\mathbf{1}]^+$ did not induce any changes in the spectrum compared to that in the presence of 2 equiv. of $CoCp_2$. These results indicate that the reducing power of $CoCp_2$ is insufficient to further reduce $[\mathbf{1HH}]^+$ even under acidic conditions.
60 The small difference in the chemical shift of the NH proton in Figure 7 and Figure 12a results from residual H_2O in the CD_3CN solvent.
61 C. White, A. Yates, P. M. Maitlis and D. M. Heinekey, *Inorg. Synth.*, 1992, **29**, 228–234.
62 G. M. Sheldrick, *Acta Crystallogr., Sect. A: Found. Crystallogr.*, 2014, **70**, C1437.
63. G. M. Sheldrick, *Acta Crystallogr., Sect. A: Found. Crystallogr.*, 2008, **64**, 112-122.

Graphical abstract

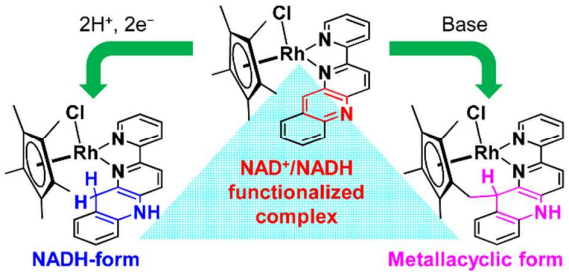

A Rh complex bearing an NAD^+/NADH-functionalized ligand undergoes different structural changes under redox or base-activated conditions.

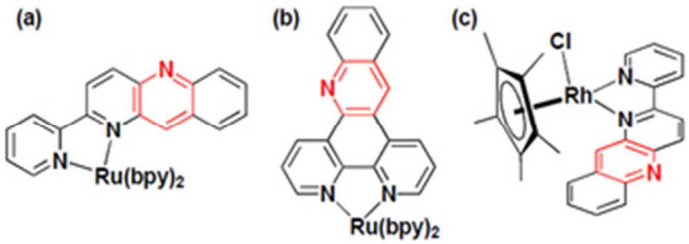

Figure 1 Metal complexes bearing NAD^+/NADH-functionalized ligands: (a) Ru-pbn, (b) Ru-bpp, and (c) $[RhCp^*(pbn)Cl]^+$ ($[\mathbf{1}]^+$).

28x10mm (300 x 300 DPI)

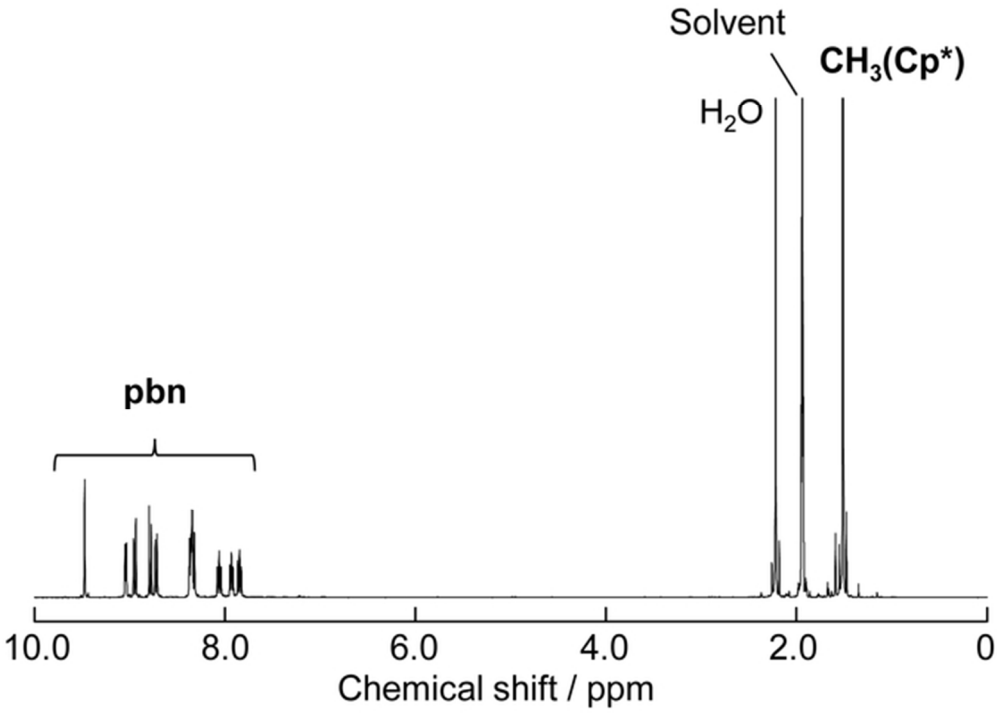

Figure 2 ^{1}H NMR spectrum of [**1**]Cl in CD_3CN.

57x40mm (300 x 300 DPI)

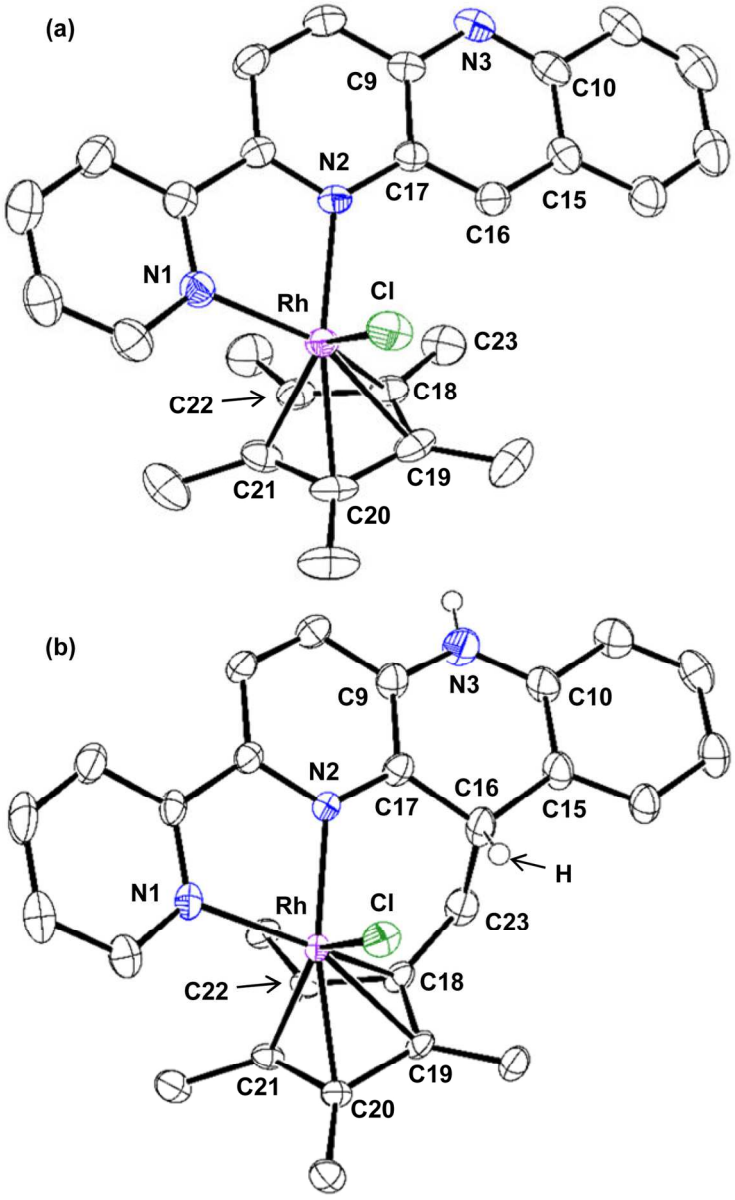

Figure 3 ORTEP drawings of [**1**][PF_6] and [**1CH**]Cl with thermal ellipsoids set to 50% probability. Counter anions, solvent molecules, and hydrogen atoms (except that of the dihydropyridine moiety in [**1CH**]Cl) are omitted for clarity.

124x199mm (300 x 300 DPI)

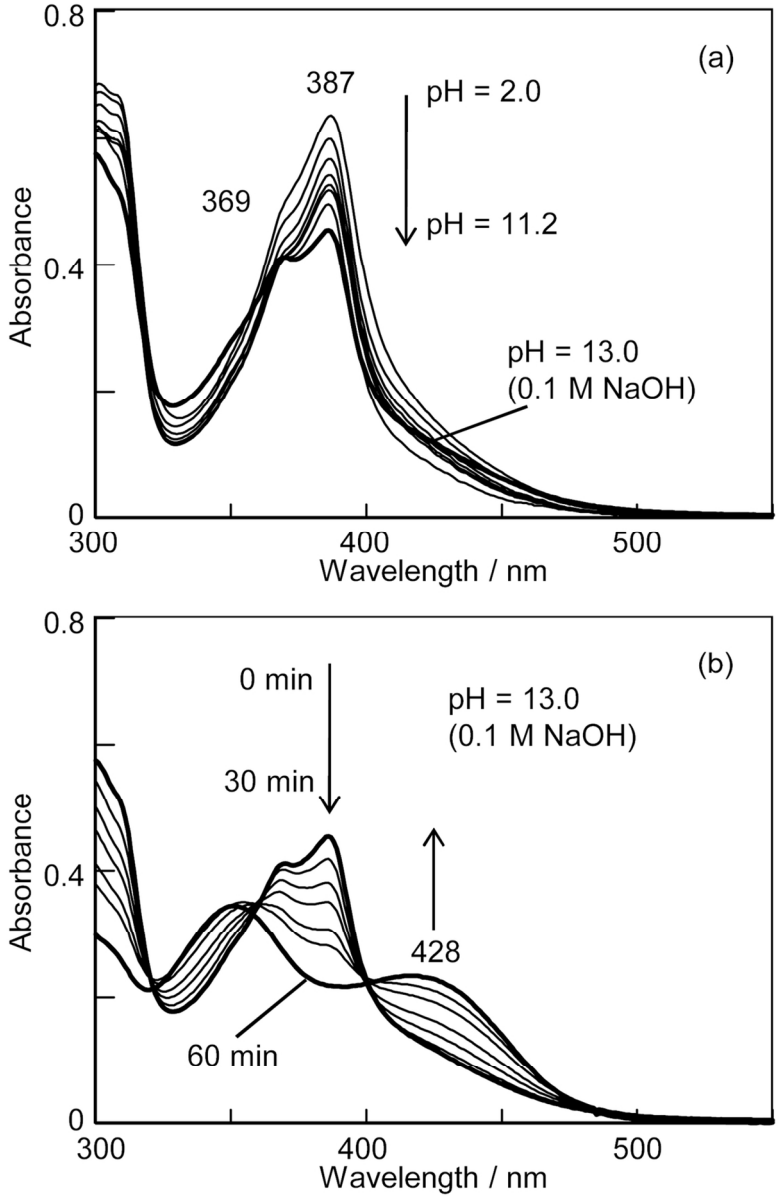

Figure 4 (a) pH-dependent and (b) time-dependent spectral changes at pH = 13.0 for [**1**]Cl in water.

97x150mm (300 x 300 DPI)

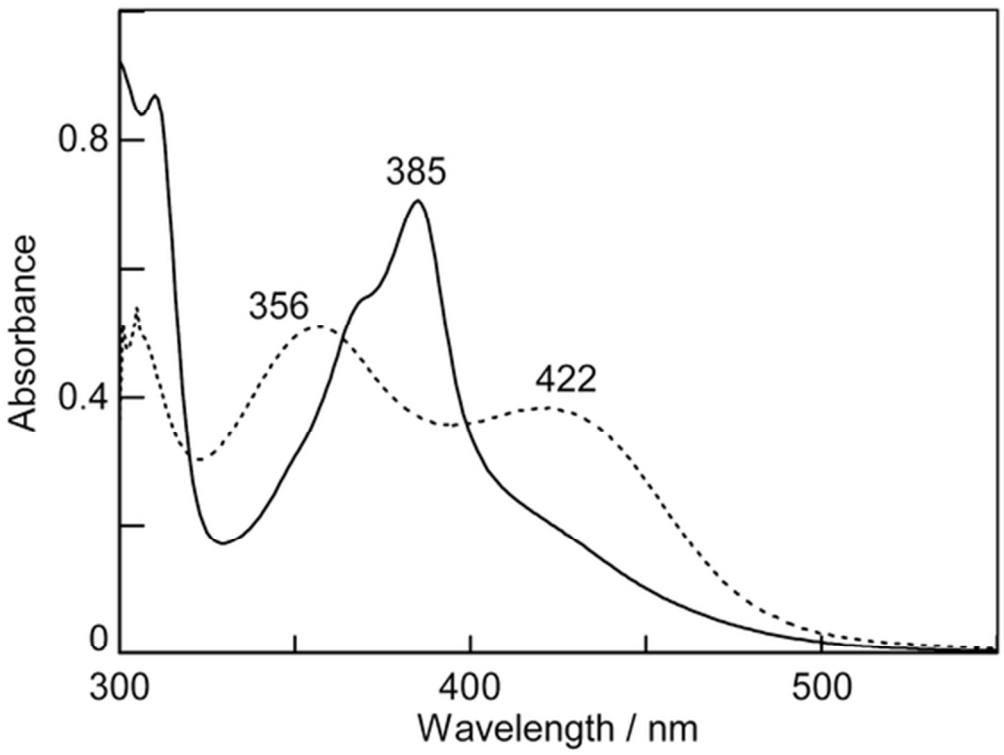

Figure 5 Electronic spectra of [**1**]Cl in CH_3CN in the absence (solid line) and presence (dotted line) of excess TEA.

49x36mm (300 x 300 DPI)

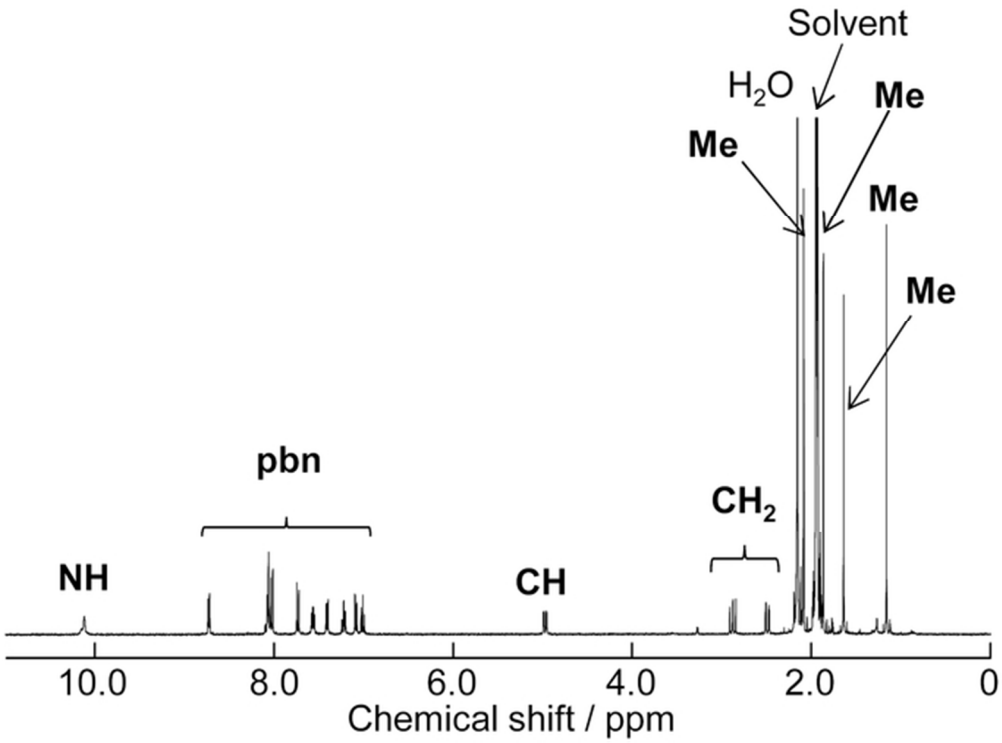

Figure 6 ^{1}H NMR spectrum of base-treated [**1**]Cl ([**1CH**]Cl).

57x42mm (300 x 300 DPI)

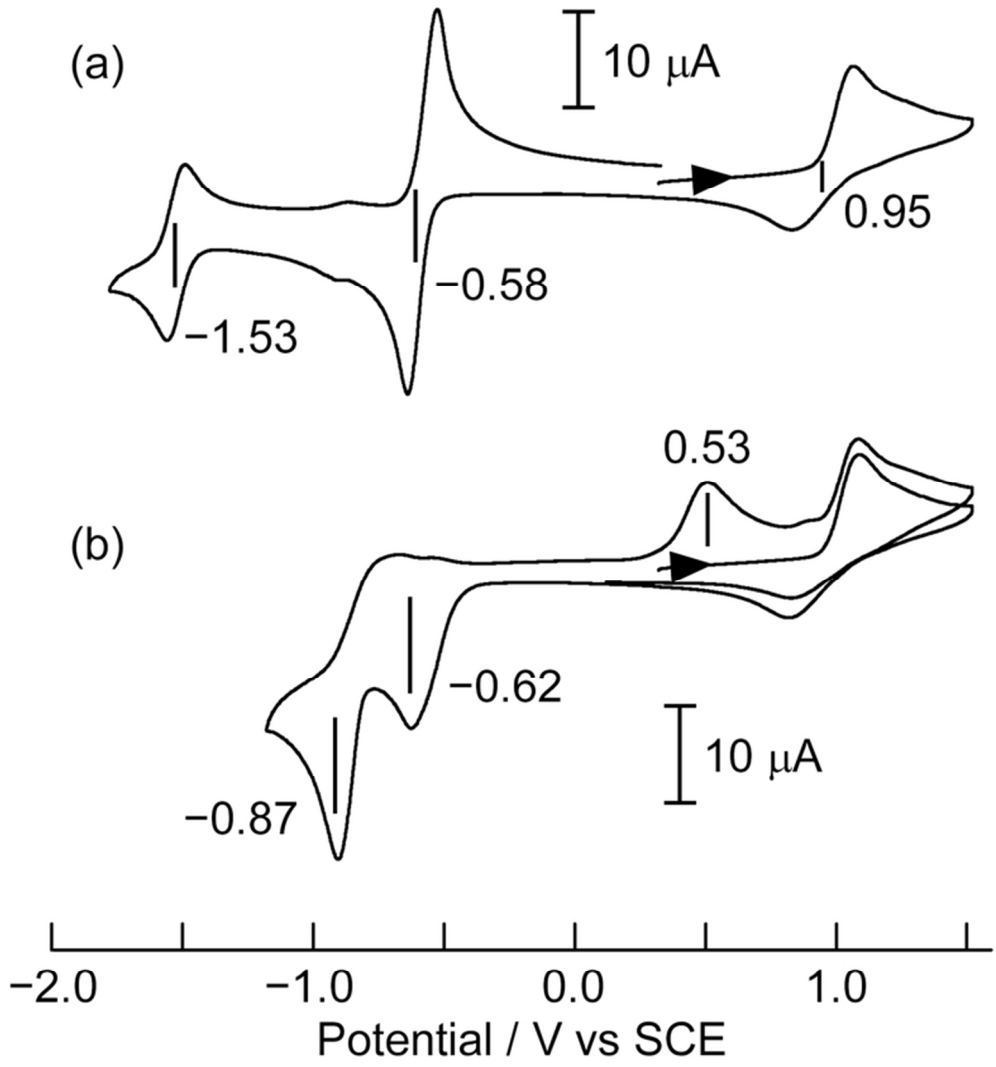

Figure 7 Cyclic voltammograms of [**1**]Cl in the (a) absence and (b) presence of 10 equiv. of AcOH in CH_3CN containing 0.1 M [nBu$_4$N][BF_4]; scan rate dV/dt = 0.1 V s^{-1}.

67x72mm (300 x 300 DPI)

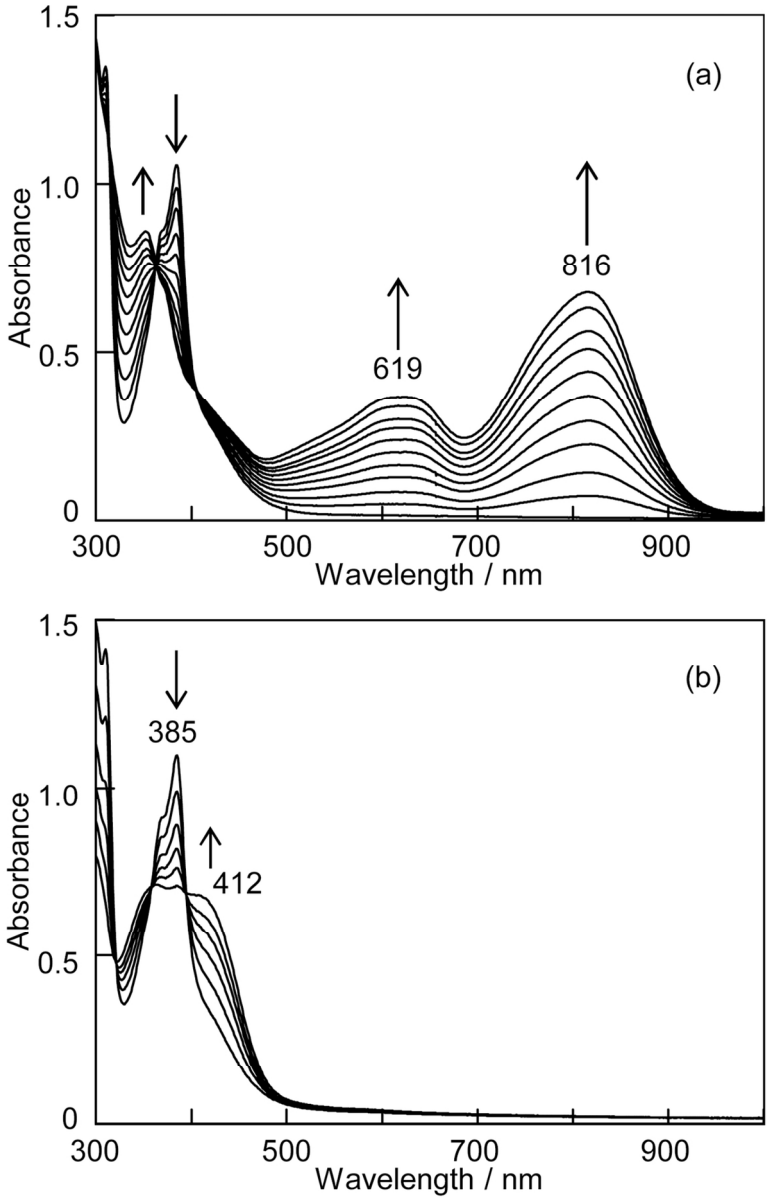

Figure 8 Spectral changes for [**1**]Cl reduced at (a) −1.0 V and (b) −0.76 V in the presence of 10 equiv. of AcOH.

98x153mm (300 x 300 DPI)

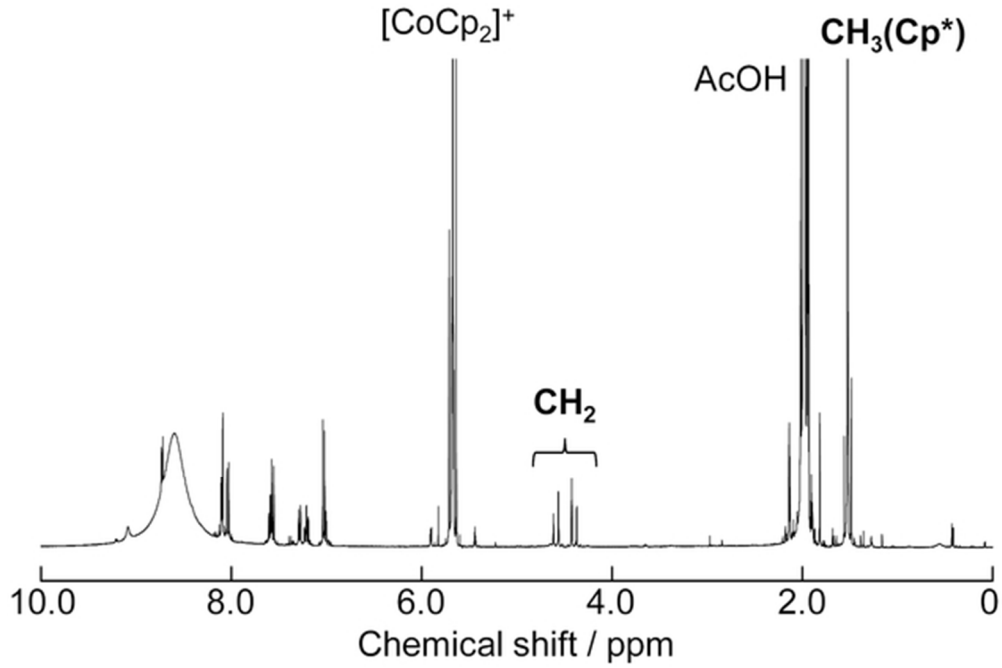

Figure 9 ^{1}H NMR spectrum of [**1**]Cl in the presence of 2 equiv. of $CoCp_2$ in CD_3CN containing 1.0% of AcOH.

53x35mm (300 x 300 DPI)

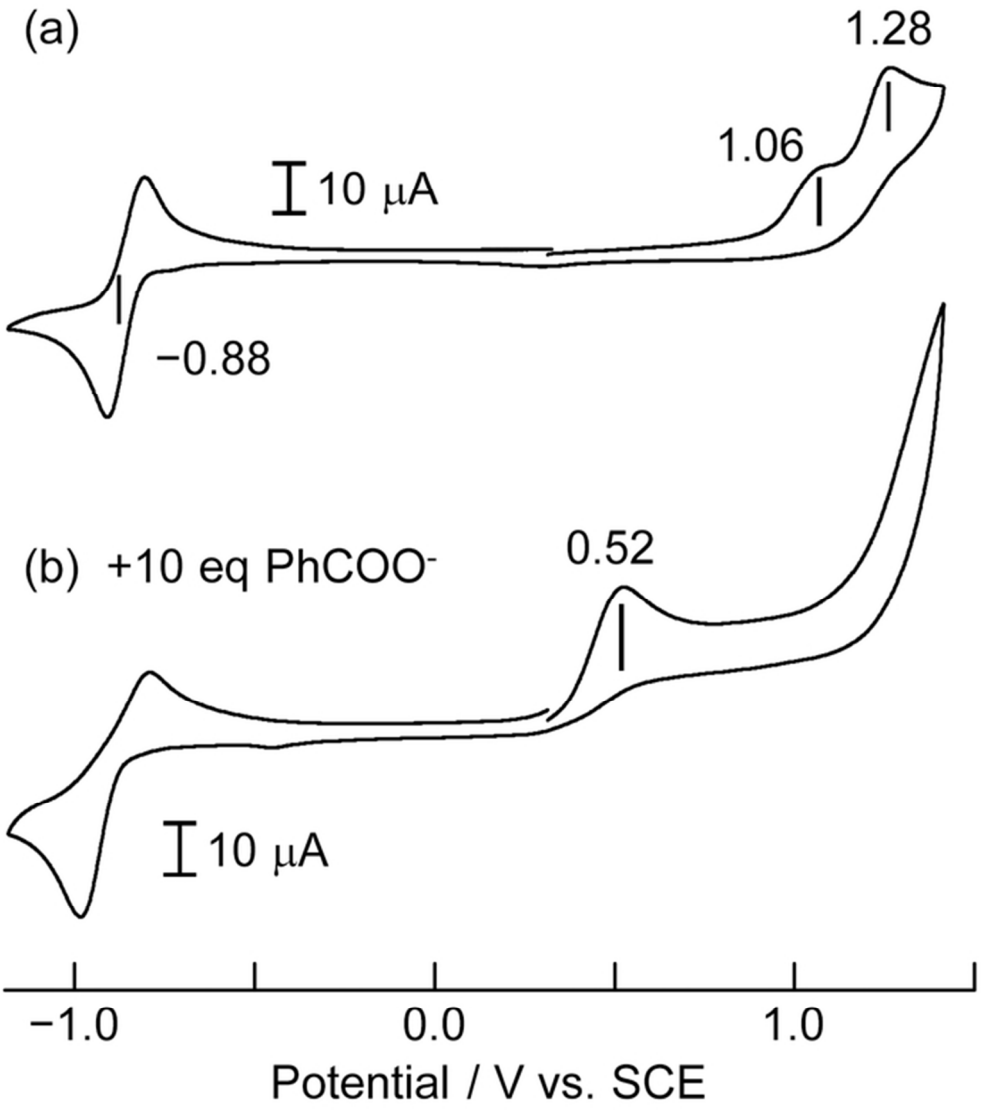

Figure 10 Cyclic voltammograms of [**1CH**]Cl in the (a) absence and (b) presence of 10 equiv. of $PhCOO^-$ in CH_3CN containing 0.1 M [nBu$_4$N][BF_4]; scan rate dV/dt = 0.1 V s^{-1}.

59x66mm (300 x 300 DPI)

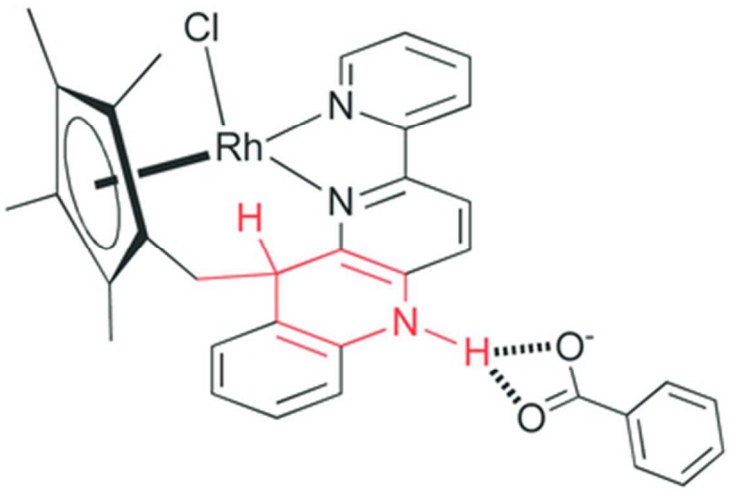

Figure 11 Predicted structure for the base adduct of [**1CH**]Cl.

31x20mm (300 x 300 DPI)

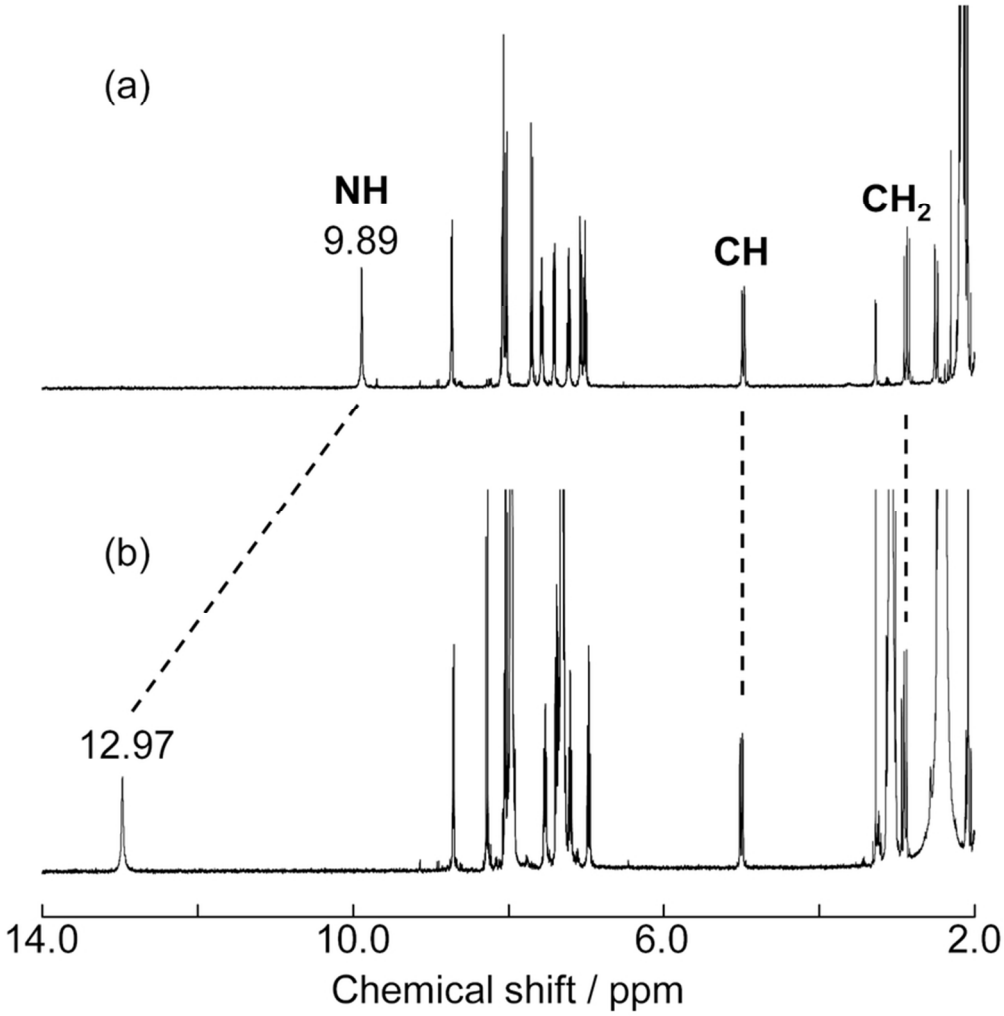

Figure 12 ^{1}H NMR changes for [**1CH**]Cl upon addition of 10 equiv. of $PhCOO^{-}$.

73x75mm (300 x 300 DPI)

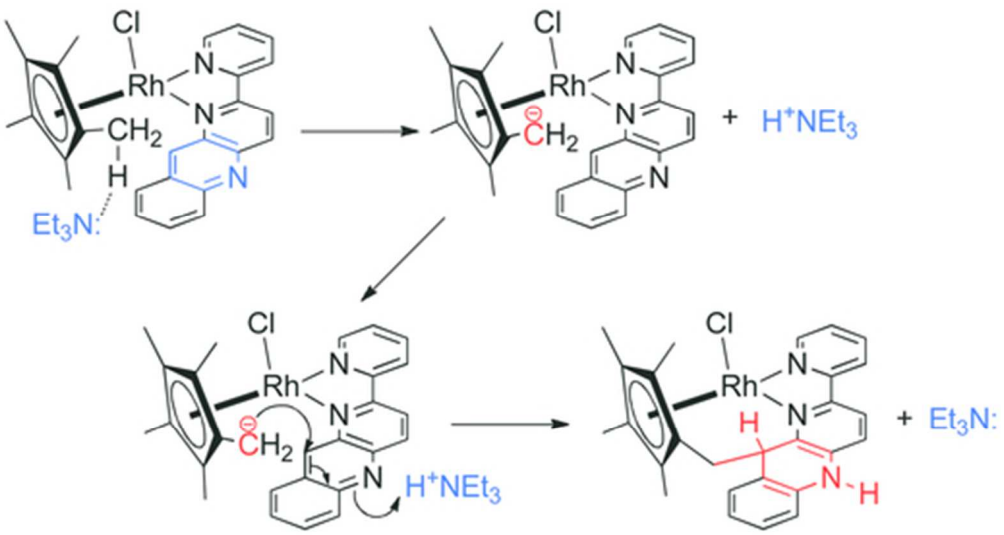

Scheme 1 Possible reaction mechanism for the generation of [**1CH**]Cl.

43x23mm (300 x 300 DPI)

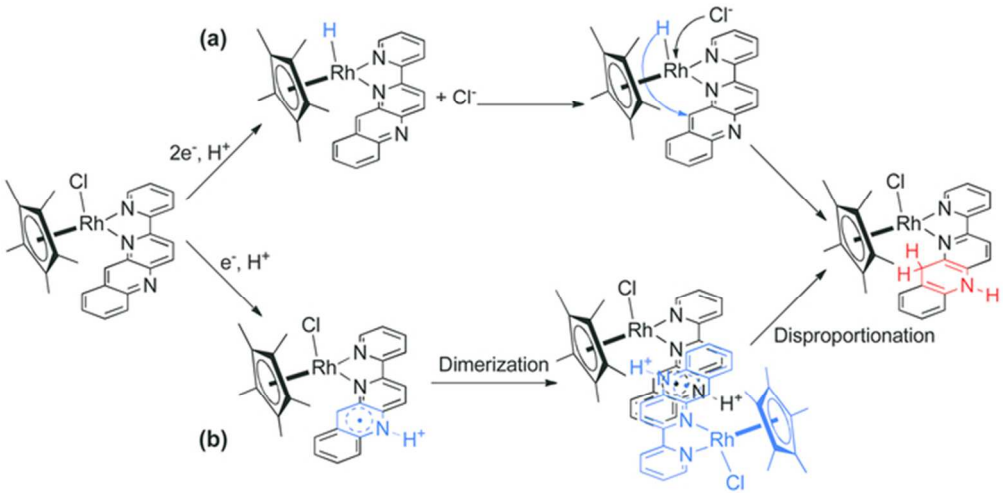

Scheme 2 Two feasible pathways for the generation of [**1HH**]$^{+}$.

60x29mm (300 x 300 DPI)